

Research Article

Influence of Incident Illumination Angle on Capacitance of a Silicon Solar Cell under Frequency Modulation

¹A. Thiam, ¹M. Zoungrana, ²H. Ly Diallo, ¹A. Diao, ¹N. Thiam, ¹S. Gueye, ¹M.M. Deme,
²M. Sarr and ¹G. Sissoko

¹Laboratory of Semiconductors and Solar Energy, Physics Department, Faculty of Science and Technology, University Cheikh Anta Diop, Dakar, Senegal

²UFR-SET, University of Thies, Senegal

Abstract: The aim of this study is to present a theoretical study of a silicon solar cell under frequency modulation. Solving the continuity equation lead to the analytical expressions of the minority carriers' density, the photocurrent and the photo voltage. The photocurrent and the photo voltage are plotted versus the modulation frequency in a semi-logarithmic scale for various incidence angles; the dynamic impedance of the solar cell is then derived. The Nyquist diagram of the impedance is plotted for various incidence angles, leading to the determination of the series and parallel resistances. The determination of the diffusion capacitance is also made based on the Bode diagram of the solar cell impedance. The influence of the modulation frequency and the incidence angle on the diffusion capacitance and the series and parallel resistances is then exhibited.

Keywords: Electrical parameters, frequency modulation, incidence angle, solar cell

INTRODUCTION

In the past, many studies were made on the n⁺-p-p⁺ silicon solar cell (Meier *et al.*, 1988) in order to improve the cell efficiency. In addition to such a literature, knowledge and understanding the intrinsic and extrinsic properties of the solar cells are fundamental in controlling the process of fabrication and treatment of semiconductors.

In this study, we consider a bifacial silicon solar cell under various incidence angles of multispectral illumination (Deme *et al.*, 2010) in frequency modulation. We study the behaviour of some electrical parameters of the bifacial solar cell, depending on the angle of incidence of polychromatic illumination. After solving the continuity equation, an expression of the excess minority carriers' density is obtained; such a step leads to the establishment and deduction of the solar cell photocurrent and photo voltage. These expressions lead to the determination of the solar cell impedance which is then studied versus modulation frequency for various incidence angles through Nyquist diagrams (Pannalal, 1973-1974; Dieng *et al.*, 2011). The series and parallel resistances are determined for various incidence angles. The solar cell capacitance is obtained by using the Bode diagram (Chenvidhya *et al.*, 2003; Ly Diallo *et al.*, 2012) also for various incidence angles and modulation frequencies.

METHODOLOGY

We present on Fig. 1 the silicon solar cell under various illumination incidence angles. *e* and *H* are respectively the emitter and the base widths, *θ* is the illumination incidence angle and *x* is the depth in the base.

Continuity equation: The continuity equation is expressed as follows:

$$D_{\omega} \cdot \frac{\partial^2 \delta(x, \theta, t)}{\partial x^2} - \frac{\delta(x, \theta, t)}{\tau} = -G(x, \theta, t) + \frac{\partial \delta(x, \theta, t)}{\partial t} \quad (1)$$

D_{ω} : The diffusion coefficient

$\delta(x, \theta, t)$: The minority carriers' density

$G(x, \theta, t)$: The generation rate depending on both time *t* and spatial coordinates *x* and *θ* the incident illumination angle (Deme *et al.*, 2010; Meier, 1988)

The minority carriers' density and the generation rate can be expressed respectively as below:

$$\delta(x, t) = \delta(x) \exp(j\omega t) \quad (2)$$

$$G(x, \theta, t) = G(x, \theta) \exp(j\omega t) \quad (3)$$

Corresponding Author: A. Thiam, Laboratory of Semiconductors and Solar Energy, Physics Department, Faculty of Science and Technology, University-Cheikh Anta Diop, Dakar, Senegal

This work is licensed under a Creative Commons Attribution 4.0 International License (URL: <http://creativecommons.org/licenses/by/4.0/>).

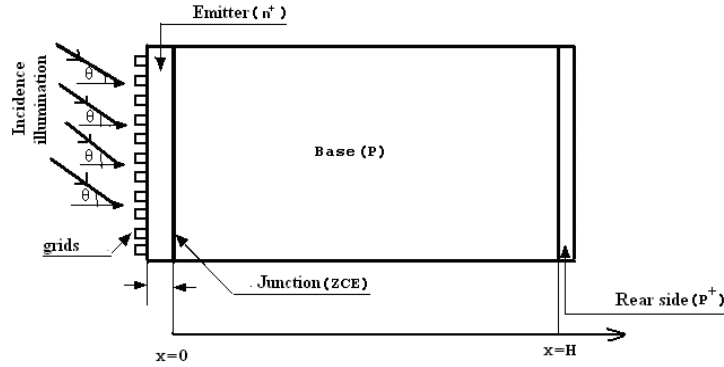


Fig. 1: Silicon solar cell

where, $\delta(x)$ is the minority carriers' density for a given depth x in the base and $G(x, \theta)$ the generation rate, a quantity depending both on spatial coordinate x and on θ , the incident illumination angle. Combining and inserting the Eq. (2) and (3) into the Eq. (1) result to the following differential equation:

$$\frac{\partial^2 \delta(x)}{\partial x^2} - \frac{\delta(x)}{L_\omega^2} = -\frac{g(x, \theta)}{D_\omega} \quad (4)$$

L_ω is the complex diffusion length.

The solution of Eq. (4) is given by the following expression:

$$\delta(x, \theta, \omega, t) = \left[Ach\left(\frac{x}{L_\omega}\right) + Bsh\left(\frac{x}{L_\omega}\right) + \sum_{i=1}^3 \frac{L_\omega^2 n \cos \theta}{D_\omega (1 - L_\omega^2 b_i^2)} a_i \exp(-b_i x) \right] \exp(j\omega t) \quad (5)$$

where, coefficients A and B are derived from the boundary conditions at the junction and at the back surface.

Boundary conditions:

- At the junction ($x = 0$)

$$\delta(x, \theta, \omega, t) = \left[Ach\left(\frac{x}{L_\omega}\right) + Bsh\left(\frac{x}{L_\omega}\right) + \sum_{i=1}^3 \frac{L_\omega^2 n \cos \theta}{D_\omega (1 - L_\omega^2 b_i^2)} a_i \exp(-b_i x) \right] \exp(j\omega t) \quad (6)$$

- At the back surface ($x = H$)

$$D_\omega \cdot \frac{\partial \delta(x, \omega, \theta)}{\partial x} \Big|_{x=H} = -S_b \cdot \delta(x, \omega, \theta) \Big|_{x=H} \quad (7)$$

where,

- Sf & Sb : The junction and back surface recombination velocities
- H : The base depth
- ω : The modulation frequency

RESULTS AND DISCUSSION

Short circuit photocurrent density: The short circuit photocurrent is obtained through the minority carriers' diffusion at the junction when $Sf > 10^4$ cm/s and its expression is as follows:

$$J_{sc} = \sum_{i=1}^3 \frac{\frac{L_\omega^2 \cdot n \cdot \cos \theta}{(L_\omega^2 \cdot b_i^2 - 1)} a_i \cdot e}{L_\omega \cdot D_\omega \cdot \cosh\left(\frac{H}{L_\omega}\right) + S_b \cdot L_\omega^2 \cdot \sinh\left(\frac{H}{L_\omega}\right)} \times \left\{ \cdot L_\omega (D_\omega \cdot b_i - S_b) \left[\cosh\left(\frac{H}{L_\omega}\right) - \exp(-b_i \cdot H) \right] + \left(b_i \cdot S_b \cdot L_\omega^2 - D_\omega \right) \sinh\left(\frac{H}{L_\omega}\right) \right\} \quad (8)$$

with: e the elementary charge Fig. 2, we present the short circuit photocurrent versus modulation frequency (semi-logarithmic scale) for various incidence angles. In Fig. 2, at the first step, for lower frequency values, the short circuit photocurrent is relatively constant before decreasing for high frequency values. At the same time, the short circuit photocurrent increases following the lower angle of incidence values; the highest current is obtained for the direct normal incidence (Sissoko *et al.*, 1992; Madougou *et al.*, 2007).

Open circuit photo voltage: The open circuit photo voltage is obtained when the junction recombination

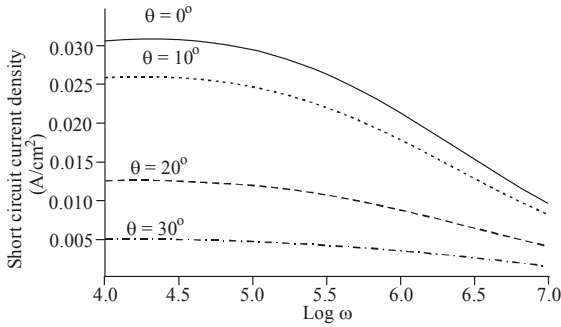


Fig. 2: Short circuit photocurrent density versus modulation frequency (semi-logarithmic scale) for various incidence angles
 D_0 : 26 cm²/s; H: 0.03 μm; τ: 4.5 10⁻⁶s; L₀: 0.02 cm

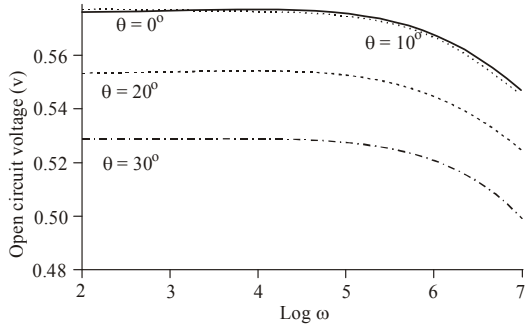


Fig. 3: Open circuit photo voltage versus modulation frequency (semi-logarithmic scale) for various incidence angles
 D_0 : 26 cm²/s; H: 0.03 μm; τ: 4.5 10⁻⁶s; L₀: 0.02 cm

velocity Sf is very low; for an ideal cell, Sf should be zero (Sf = 0) and in a real case, it would be the intrinsic junction recombination Sf₀ (Diallo *et al.*, 2008).

In our case (Sf = 0), its expression is given by:

$$V_{oc} = V_T \cdot \ln \left(1 + \sum_{i=1}^3 \left[\frac{\left[\frac{N_b}{n_0^2} \cdot \frac{L_\omega^2 \cdot n \cdot \cos \theta}{L_\omega^2 \cdot b_i^2 - 1} \cdot a_i \right]}{\left[L_\omega \cdot D_\omega \cdot Sb \cdot \cosh \left(\frac{H}{L_\omega} \right) + D_\omega^2 \cdot \sinh \left(\frac{H}{L_\omega} \right) \right]} \right] \times \left[-L_\omega (Sb - D_\omega \cdot b_i) \left[\cosh \left(\frac{H}{L_\omega} \right) - \exp(-b_i \cdot H) \right] + \left[L_\omega^2 \cdot b_i \cdot Sb - D_\omega \right] \sinh \left(\frac{H}{L_\omega} \right) \right] \right] \right) \quad (9)$$

The Fig. 3 shows a plot of the open circuit photo voltage versus modulation frequency in semi logarithmic scale.

Solar cell impedance: The dynamic impedance of the solar cell can be expressed as:

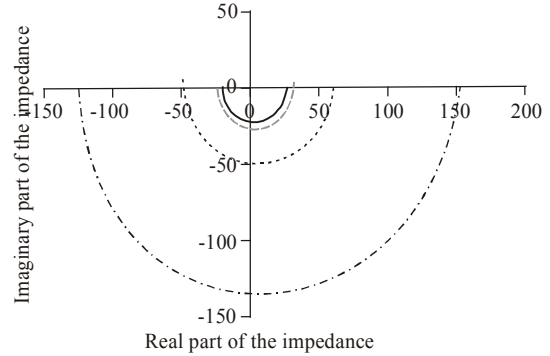


Fig. 4: Imaginary part versus real part of the solar cell impedance for different incidence angles
 Sf : 3.10³ cm/s; D_0 : 26 cm²/s; H: 0.03 μm; τ: 4.5 10⁻⁶s; L₀: 0.02 cm

$$Z(\omega, \theta, Sf) = \frac{V(\omega, \theta, Sf)}{J(\omega, \theta, Sf)} \quad (10)$$

The NYQUIST diagram (imaginary part versus real part) of solar cell dynamic impedance Z (Honma and Munakata, 1987; Pereira *et al.*, 2006) is plotted (Fig. 4) for various incidence angles. The Nyquist plot of impedance is a semi-circle.

These curves show that the locus of the semi-circle increases with increasing incidence angle. Series and parallel resistances Rs and Rp are deduced from the above Nyquist diagram (Honma and Munakata, 1987; Pereira *et al.*, 2006; Bouzidi *et al.*, 2007) given that the two intercepts of the impedance locus on the real axis are approximately Rs and Rs + Rp (Bashahu and Habyarimana, 1995; El-Adawi, 2002).

From Fig. 5, series and parallel resistances are extracted for various incidence angles and presented on Table 1.

Table 1 show that the series and parallel resistances increase with the incidence angle.

Once these parameters are determined, we can use the Bode diagram to access to the cut-off angular frequency and finally the capacitance.

Solar cell diffusion capacitance: The diffusion capacitance C associated to the minority carriers' collection region is related to the cut-off angular frequency ω_c by:

$$R_p \cdot C = \frac{2 \cdot \pi}{\omega_c} \quad (11)$$

Bode diagram: Here, Bode diagram (Pannalal, 1973-1974) is used to access to the cut-off frequency; we present on the Fig. 4 the Bode diagram of the solar cell impedance for various incidence angles.

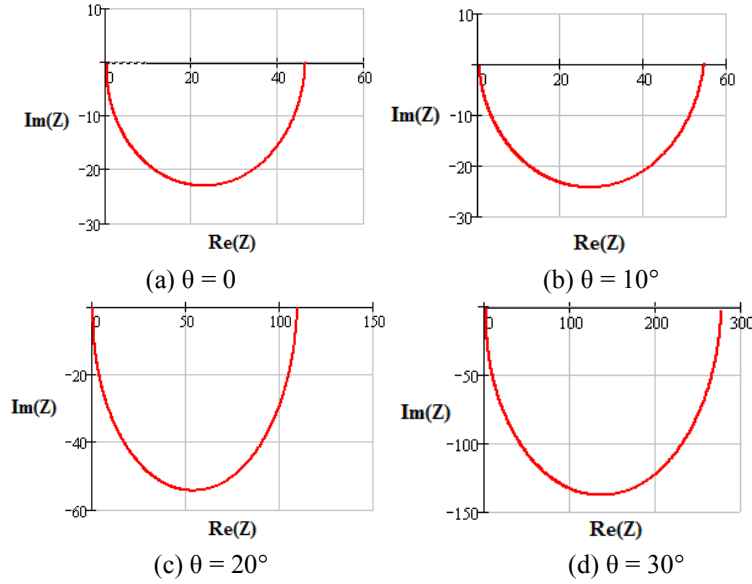


Fig. 5: Nyquist diagram of the dynamic impedance for various incidence angles
 Sf: $3 \cdot 10^3$ cm/s; D_0 : $26 \text{ cm}^2/\text{s}$; H : $0.03 \text{ }\mu\text{m}$; τ : $4.5 \cdot 10^{-6}$ s; L_0 : 0.02 cm

θ ($^\circ$)	0	10	20	30
R_s ($\Omega \cdot \text{cm}^2$)	0.282	0.566	1.310	2.790
R_p ($\Omega \cdot \text{cm}^2$)	21.41	36.23	54.37	196.7

θ ($^\circ$)	0	10	20	30
θ ($^\circ$)	0	10	20	30

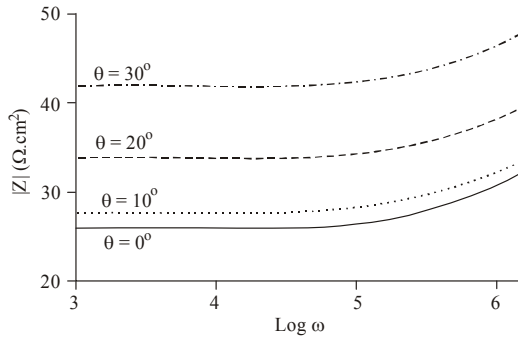


Fig. 6: Bode diagram of the impedance for various incidence angles
 Sf: $3 \cdot 10^3$ cm/s; D_0 : $26 \text{ cm}^2/\text{s}$; H : $0.03 \text{ }\mu\text{m}$; τ : $4.5 \cdot 10^{-6}$ s; L_0 : 0.02 cm

For angular frequencies in the interval $0 < \omega < \omega_c$, the impedance is independent of the frequency: that is we are still in a quasi-steady state. For the values of the pulsation such as $\omega > \omega_c$ the impedance increases with the angular frequency. Effectively for frequency above ω_c , minority carriers are slowed down traducing the fact that the dynamic impedance increases.

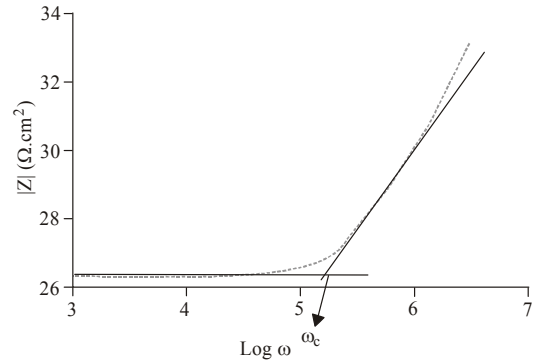


Fig. 7: Bode diagram of the impedance
 Sf: $3 \cdot 10^3$ cm/s; D_0 : $26 \text{ cm}^2/\text{s}$; H : $0.03 \text{ }\mu\text{m}$; τ : $4.5 \cdot 10^{-6}$ s; L_0 : 0.02 cm

We also note that all the curves in Fig. 6 present a knee at approximately the same angular frequency that is, the angular cut-off frequency do not depend on the incidence angle. Since the curves in Fig. 6 lead to the same cut-off angular frequency for any incidence angle, we finally consider Fig. 7 ($\theta = 0^\circ$) for the determination of ω_c .

Figure 7 shows the determination of the angular cut-off frequency. Approximately, we have:

$$\omega_c = 13 \cdot 10^4 \text{ rad/s} \tag{12}$$

Since the parallel resistance has been already determined, based on the angular cut-off frequency above we can deduce the capacitance value for various incidence angles; the results are presented on Table 2.

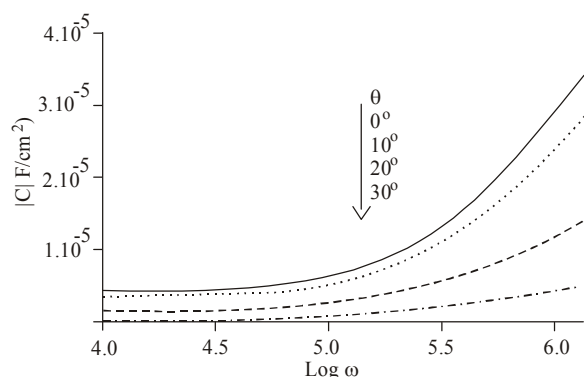


Fig. 8: Bode diagram of the capacitance for various incidence angles

Sf: $3 \cdot 10^3$ cm/s; D_0 : 26 cm²/s; H: 0.03 μm, τ : $4.5 \cdot 10^{-6}$ s; L_0 : 0.02 cm

This table shows that the capacitance decreases with increasing incidence angle.

To confirm such a result, let us express the capacitance as follow:

$$C = \frac{e^2}{K \cdot T} \left(\frac{n_0^2}{N_b} + \delta(0) \right) \quad (13)$$

Based on this expression, we now plot on Fig. 8 the capacitance of the cell versus modulation frequency in semi-logarithmic scale (Bode diagram).

This figure shows that the capacitance increases with increasing modulation frequency for a given incidence angle; that is, when modulation frequency increases, minority carriers are stored more and more in the base because they cannot cross the junction; this lead to an increase in the capacitance of the cell.

We also note that the capacitance decreases with increasing incidence angle as previously noted on Table 2.

Effectively, when the incidence angle increases, there is less and fewer carriers generated in the base leading to a decrease of the net charge in the base and thus a decrease in the capacitance associated to the cell.

CONCLUSION

A theoretical study is made on a silicon solar cell under the frequency modulation for various incidence illumination angles. The photocurrent and the photo voltage are studied and the influence of the modulation frequency and incidence angle are presented. The solar cell dynamic impedance is presented and leads to the determination of the series and parallel resistances through Nyquist diagrams. The angular cut-off

frequency is determined by use of Bode diagram of the dynamic impedance and the capacitance is deduced based on both parallel resistance and angular cut-off frequency; the capacitance determined by this way decreases with increasing incidence angle. This behaviour of the capacitance is confirmed by using an analytical expression of the solar cell capacitance.

REFERENCES

- Bashahu, M. and A. Habyarimana, 1995. Review and test of methods for determination of the solar cell series resistance. *Renew. Energ.*, 6(2): 127-138.
- Bouzidi, K., M. Chegaar and A. Bouhemadou, 2007. Solar cells parameters evaluation considering the series and shunt resistance. *Solar Energ. Mater. Solar Cells*, 91: 1647-1651.
- Chenvidhya, D., K. Kirtikara and C. Jivacate, 2003. A new characterization method for solar cell dynamic impedance. *Solar Energ. Mater. Solar Cells*, 80(4): 459-464.
- Deme, M.M., S. Mbodji, S. Ndoye, A. Thiam, A. Dieng and G. Sissoko, 2010. Influence of illumination incidence angle, grain size and grain boundary recombination velocity on the facial solar cell diffusion capacitance. *Revue des Energ. Renouvelab.*, 13(1): 109-121.
- Diallo, H.L., A.S. Maiga, A. Wereme and G. Sissoko, 2008. New approach of both junction and back surface recombination velocities in a 3D modeling study of a polycrystalline silicon solar cell. *Eur. Phys. J. Appl. Phys.*, 42: 193-211.
- Dieng A., N. Thiam, A. Thiam, A.S. Maiga and G. Sissoko, 2011. Magnetic field effect on the electrical parameters of a polycrystalline silicon solar cell. *Res. J. Appl. Sci. Eng. Technol.*, 3(7): 602-611.
- El-Adawi, M.K. and I.A. Al-Nuaim, 2002. A method to determine the solar cell series resistances from a single I-V characteristic curve considering its shunt resistance-new approach. *Vaccum.*, 64: 33-36.
- Honma, N. and C. Munakata, 1987. Sample thickness dependence of minority carrier lifetimes measured using an ac photovoltaic method. *Japanese J. Appl. Phys.*, 26(12): 2033-2036.
- Ly Diallo, H., M. Wade, I. Ly, M. Diaye, B. Dieng, O.H. Lemrabott, A.S. Maiga and G. Sissoko 2012. 1D modeling of a bifacial silicon solar cell under frequency modulation monochromatic illumination: Determination of the equivalent electrical circuit related to the surface recombination velocity. *Res. J. Appl. Sci. Eng. Technol.*, 4(12): 1672-1676.

- Meier, D.L., J.M. Hwang and R.B. Cambell, 1998. The effect of doping density and injection level on minority-carrier lifetime as applied to bifacial dendritic web silicon solar cells. *IEEE Trans. Electr. Dev.*, 35(1): 70-79.
- Madougou, S., F. Made, M.S. Boukary and G. Sissoko, 2007. Recombination parameters by using Internal Quantum Efficiency (IQE) data of bifacial solar cell. *Adv. Mater. Res.*, 18-19: 313-324.
- Pannalal, L. and B. Signals, 1973-1974. *Systems and Controls*. Intext Educational Publisher, New York.
- Pereira, L., L. Raniero, P. Barquinha, E. Fortunato and Martins, 2006. Impedance study of the electrical properties of poly-Si thin film transistors. *J. Non-Cryst. Solids*, 352(9-20): 1737-1740.
- Sissoko, G., S. Sivoththanam, M. Rodot and P. Mialhe, 1992. Constant Illumination-Induced Open Circuit Voltage Decay (CIOCVD) method, as applied to high efficiency Si Solar cells for bulk and back surface characterization. 11th European Photovoltaic Solar Energy Conference and Exhibition, poster 1B, 12-16, pp: 352-354.